Journal of Applied Fluid Mechanics, Vol. 11, No. 2, pp. 447-457, 2018.
Available online at www.jafmonline.net, ISSN 1735-3572, EISSN 1735-3645.
DOI: 10.29252/jafm.11.02.27527

Snap-Off Criteria for Dynamic Flow Conditions in Constricted Circular Capillaries

J. A. Quevedo Tiznado[1], C. Fuentes[2†], E. González Sosa[1] and C. Chávez[1]

[1] *Faculty of Engineering, Autonomous University of Queretaro, Querétaro, Qro., Mexico*
[2] *Mexican Institute of Water Technology, Jiutepec, Morelos, Mexico*

†*Corresponding Author Email: cbfuentesr@gmail.com*

(Received December 21, 2016; accepted October 5, 2017)

ABSTRACT

One of the main mechanisms of emulsion formation in porous media is the snap-off; invasion of the wetting phase flowing adjacent to the pore wall within a constriction mostly occupied by the non-wetting phase, causing breakup into isolated drops of this phase. The current approaches to determine the occurrence of this phenomenon have been formulated for quasistatic flow conditions, where the mechanisms governing the flow are controlled by the geometry of the capillary. However, some studies suggest that the drop breakup does not occur above a capillary number threshold and given a certain viscosity ratio, even if the static breakup criteria are met. In this paper, we extend the current numerical analysis of the capillary number upper limit (Ca_{lim}), in which the snap-off is inhibited, by considering the effect of viscosity ratio on the dynamics of immiscible two-phase flow through constricted circular capillaries. Based on the results of this study, empirical mathematical expressions that relate the main physical variables of the flow were established as breakup criteria for dynamic flow conditions. The dynamic breakup criteria takes into account, jointly: some aspects of rheology of the two-phase system, such as the viscosity ratio; the dynamic factors of the flow, encapsulated in the local capillary number; and an integral form of the capillary geometry, represented by a parameter that relates both radii and the distance between them.

Keywords: Drop breakup; Pore-scale flow; Local capillary number; Capillary geometry.

NOMENCLATURE

a	radii ratio
(b, m)	fitting parameters of the linear regression
(A, B, C, D)	fixed fitting parameters
Ca	local capillary number
Ca_{lim}	local capillary number upper limit
$Ca_{lim}^{\tilde{\alpha}}$	values of Ca_{lim} grouped by $\tilde{\alpha}$
Ca_{lim}^{k}	values of Ca_{lim} grouped by k
E	objective function for fixed parameters
$E1$	objective function for variable parameters
(d, e, f, g)	variable fitting parameters
k	viscosity ratio
ℓ	capillary length
L	dimensionless capillary length
P	flow pressure
P_c	capillary pressure
Q	total volumetric flow
r	radial coordinate
R_g	capillary constriction radius
R_T	capillary radius
t	time
u	axial velocity
x	axial coordinate
α	pore wall slope
$\tilde{\alpha}$	pore geometric gradient
δ	wetting film thickness
κ	interface radius
λ	pore wall coordinate
μ	dynamic viscosity
σ	surface tension
τ	dimensionless time
τ_s	dimensionless snap-off time

Subscripts

1	non-wetting phase
2	wetting phase

Superscripts

*	dimensionless variable

1. INTRODUCTION

Adequate knowledge of the multiphase flow at pore-scale is of vital importance for oil production (Blunt *et al*. 2013). In the reservoirs, the movement of water, gas and oil is presented simultaneously in a complex system of pores and throats. During the secondary oil recovery process, a clear example of this multiphase flow occurred. It involved the introduction of water by injection wells, to displace and recover fluids trapped in the reservoir towards production wells. Similar conditions are presented in a group of enhanced oil recovery methods, called "smart waterflooding", in which the chemical design of the injected water is modified to increase oil recovery (Alvarado *et al*. 2014). However, these flow conditions, where there is an interaction between the different phases, prove to be favorable for the formation of some dispersion types within the porous media. These, if not controlled, can negatively affect the production.

Dispersion is a two-phase system constituted by one phase that is dispersed in a second phase, thereby called continuous. There are different types of dispersions with a liquid as a continuous phase. Based on the nature of the dispersed phase, dispersions can be of three types: foams (gaseous), emulsions (liquid) and suspensions (solid). Here we focus on emulsions (liquid-liquid dispersion), which unlike foams, the viscosity of the dispersed phase is not negligible, and is important in their characterization (Kokal, 2005).

Depending on the circumstances, the formation of emulsions within the porous media can help or hinder the oil recovery. For instance, emulsion drops can block some pore clusters and thus divert the flow to unswept areas allowing residual oil to be mobilized (Cobos *et al.* 2009; Romero *et al.* 2011 Guillén *et al.* 2012a; Guillén *et al.* 2012b). On the other hand, the formation of uncontrolled emulsions in oil production entails several operational problems and increases production costs. In order to meet crude oil transport specifications in downstream facilities, produced emulsions have to be treated. Through this treatment, water and associated inorganic salts removal takes place; as well as corrosion reduction (Peña *et al.* 2009).

Emulsions in the porous media can be formed during the immiscible two-phase flow when the non-wetting phase loses continuity by generating droplets. One of the main mechanisms responsible for emulsification is the so-called snap-off; invasion of the wetting phase flowing adjacent to the pore wall within a constriction mostly occupied by the non-wetting phase, causing breakup into isolated drops of this phase. The current approaches for determining the occurrence of this phenomenon have been formulated for quasistatic flow conditions, where the mechanisms governing flow are controlled by the capillary geometry. Roof (1970) was the first to propose a criterion for snap-off occurrence in constricted capillaries, consisting of a relationship between the major and minor radii of the capillary. This criterion is based on the analysis of the capillary pressure and considers that the pressure in the continuous phase is constant throughout the geometry of the capillary. The Roof criterion has been used in studies related to foam generation by snap-off in porous media (Kovscek and Radke, 1996). However, there is a controversy in trying to explain under what conditions snap-off occurs or is inhibited (Rossen, 2000; Kovscek and Radke, 2003; Kovscek *et al.* 2007; Rossen, 2008). Beresnev *et al*. (2009) introduced the wavelength of the capillary in a new geometric breakup criterion based on a detailed analysis of the pressure gradients of both phases inside the capillary. The validity of this criterion was examined using a mathematical model that describes the temporal evolution of the interface in liquid-liquid two-phase flow system and both microfluidic and computational fluid dynamics experiments (Beresnev and Deng, 2010; Beresnev *et al*. 2011a).

Recently, in a numerical study Deng *et al*. (2015) prove the existence of an upper limit of the local capillary number in which snap-off is inhibited, even if the geometric breakup criteria are met (for example that of Beresnev *et al*. 2009). Although a broad range of geometries was covered in the study of Deng *et al*. (2015), their analysis has been limited to the study of a system where the viscosity ratio was equal to unity. Furthermore, these authors attribute the snap-off inhibition to the critical conditions that arise due to the presence of fast flow in the pores, related to the local capillary number increases, which prevent the growth of the wetting film in the pore constriction.

Similarly, Peña *et al*. (2009) based their study on a simple theoretical model and their microfluidic experimental results. They found that the occurrence or inhibition of the snap-off was not only governed by the capillary number, but also it was influenced by the viscosity ratio. Additionally, it was observed that a high viscosity of the non-wetting phase suppresses the drop breakup, whereas in low viscosities this always occurred. Moreover, snap-off was observed only at low capillary numbers at moderate viscosities ratios. These authors relate the breakup time and snap-off occurrence with the flow of the continuous phase towards the constriction, and establish that this flow is affected by the interaction of three forces acting competitively: the capillary pressure difference that drives the wetting phase to constriction, the resistance to the flow of the wetting liquid and the squeezing process of the non-wetting phase.

In this context, it is pertinent to have a breakup criterion that takes into account, jointly, the parameters that adequately describe the geometry of the capillary (geometric slope, wavelength, radii ratio), dynamic flow factors (local capillary number), and some aspects of the rheology of the two-phase flow system (viscosity ratio). This study examined numerically the behavior of the local capillary number upper limit to identify the inhibition of snap-off, for different geometry configurations of constricted circular capillaries and viscosity ratios. Moreover, empirical mathematical expressions were established to relate these

variables, which can serve as breakup criteria for dynamic flow conditions. A new variable, the geometric gradient $\tilde{\alpha}$ has been introduced in this work, which integrally relates the main parameters of the geometric breakup criteria; namely, the wavelength (Beresnev *et al.* 2009) and the radii ratio of the capillary (Roof, 1970). The research is based on the dynamics of the two-phase flow described by the model proposed by Beresnev and Deng (2010). This model is derived from the simplified incompressible Navier-Stokes equations, conservation of mass and continuity principles, and Young-Laplace equation. The model consisted of a nonlinear fourth order partial differential equation that was solved with the "Method of Lines" framework implemented in MATHEMATICA® (Knapp, 2008).

This article is divided in four parts. In section 2 called methods, the geometry of the problem is presented. Later, the governing equations are exposed in order to derive the snap-off model. Following, the model is evaluated for different cases in which the geometrical parameters, the viscosity ratio, and the capillary number are varied. For each case, the capillary number upper limit and the snap-off time are determined. Afterwards, section 3 includes the results of applied empirical formulations that are proposed to predict the Ca_{lim}. Right after, discussion takes place. Finally, conclusions and some recommendations are provided in section 4.

2. METHODS

2.1 Snap-Off Geometry

The porous structure of a reservoir presents complex geometric shapes; among these, the presence of constrictions in the capillary channels called pore throats is found. This basic geometry of the porous medium, consisting of a capillary with one or more constrictions, has been used to study the mechanism of drop breakup during the immiscible two-phase flow at pore-scale. During this type of flow, the pores have preference to be wetted by one of the phases, either water or oil; whereby one layer of the wetting phase will be present between the pore-wall and the non-wetting phase. The schematic of the fluid configuration is given by Fig.1:

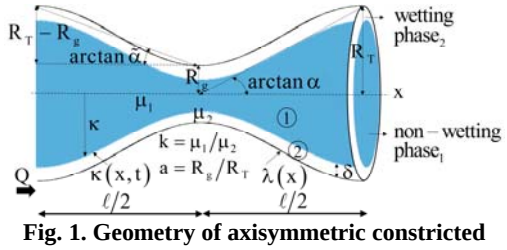

Fig. 1. Geometry of axisymmetric constricted capillaries and configuration of the liquid phases.

The following sinusoidal function was used to represent the geometry of axisymmetric capillaries with constriction:

$$\lambda(x) = 0.5R_T\left[(1+a)-(1-a)\cos\left(\alpha\pi x/R_T\right)\right] \quad (1)$$

where λ is the radial coordinate of the capillary wall, x refers to the axial coordinate, a is the ratio between the throat (R_g) and capillary (R_T) radii, and α is a geometric parameter which represents the ratio between the capillary radius (R_T) and half of the capillary length (ℓ), $\alpha=R_T/(\ell/2)$, as shown in Fig. 1. The parameter α, also called pore wall slope (Gauglitz and Radke, 1990; Beresnev and Deng, 2010), does not consider the throat radius. Therefore, it does not totally represent the capillary geometry. Here, we introduce the dimensionless parameter $\tilde{\alpha}$ that relates the wavelength and both radii of the form $\tilde{\alpha}=(R_T-R_g)/(\ell/2)$, and represents the geometric gradient of the pore wall (see Fig. 1). Thus, the sinusoidal function [Eq. (1)] results in the next equation:

$$\lambda(x) = 0.5R_T\left\{(1+a)-(1-a)\cos\left[\frac{\tilde{\alpha}\pi x}{(1-a)R_T}\right]\right\} \quad (2)$$

2.2 Governing Equations

To simulate the drop breakup process in capillaries, the mathematical model developed by Beresnev and Deng (2010) was applied. This model is based on the equation of conservation of mass in the "small-slope" approximation [$\alpha=R_T/(\ell/2)\ll 1$] for arbitrary viscosities of the fluids and the presence of an imposed base flow.

The small-slope approximation (Gauglitz and Radke, 1990) assume the smallness of the capillary and Reynolds numbers, which allows to approximate the fluid flow in the capillary as a Poiseuille flow. According to the obtained results to verify the limits of validity of this model through both microfluidic and computational fluid dynamics experiments (Beresnev and Deng, 2010; Beresnev *et al.* 2011a), it was proved that the smaller the pore wall slope α and the capillary number, the better the small-slope approximation is.

The basic equations for the model are the simplified incompressible Navier-Stokes, conservation of mass, continuity and Young-Laplace equations:

$$-\frac{\partial P_{1,2}}{\partial x}+\mu_{1,2}\frac{1}{r}\frac{\partial}{\partial r}\left(r\frac{\partial u_{1,2}}{\partial r}\right)=0 \quad (3)$$

$$\left(\frac{\partial Q_1}{\partial x}\right)dx=-2\pi {R_T}^2\kappa\left(\frac{\partial \kappa}{\partial t}\right)dx \quad (4)$$

$$Q_1+Q_2=Q \quad (5)$$

$$P_c=P_1-P_2=\sigma\left(\frac{1}{\kappa}-\frac{\partial^2\kappa}{\partial x^2}\right) \quad (6)$$

or in differential form (solving for $\partial P_1/\partial x$):

$$\frac{\partial P_1}{\partial x}=\frac{\partial P_2}{\partial x}-\sigma\left(\frac{1}{\kappa^2}\frac{\partial \kappa}{\partial x}+\frac{\partial^3\kappa}{\partial x^3}\right) \quad (7)$$

where P is the pressure, subscripts 1 and 2 denote , respectively, the non-wetting and wetting phase, μ is dynamic viscosity, r the radial coordinate, u is the axial velocity, t the temporal variable, Q the total volume flux of both fluids through the capillary, P_c is the capillary pressure, κ the radius of interface and σ the surface tension. The volume flux, defined as $Q=2\pi\int(u)rdr$, is related to the local capillary number, which links the competition between the viscous and capillary forces, through the expression $Ca=(Q/\pi R_T^2)\mu_2/\sigma$, where the term in parentheses refers to the average velocity of the local flow in the capillary.

The drop breakup problem needs to determine the interface position change over time. The equation pair (one for each phase) that is derived from Eqs. (3), (4), (5), and (7), and the definition given of the volume flux applied in each phase, form a seven-equation system which unknowns are P_1, P_2, u_1, u_2, Q_1, Q_2, and κ. Instead of solving this equation system, Beresnev and Deng (2010) derive an evolution equation to describe the free liquid-liquid dynamic interface from the mass conservation expression, Eq. (4), which can be re-written as:

$$\frac{\partial \kappa}{\partial t}=\frac{1}{-2\pi R_T{}^2\kappa}\left(\frac{\partial Q_1}{\partial x}\right) \tag{8}$$

In order to close the evolution equation, the volume flux of the non-wetting phase Q_1 requires to be explicitly expressed through the interface position κ. Then, first, Eq. (3) is analytically solved for each phase with the following boundary conditions: 1) non-slip on the wall 2) equilibrium of both the shear stress and from the velocities at the interface. As a result, the axial velocities are obtained. By integrating the velocities between the corresponding limits, the volume flux in each phase is obtained:

$$Q_1=2\pi\int_0^{\kappa}u_1rdr=-\frac{\pi\kappa^4}{8\mu_1}\frac{\partial P_1}{\partial x}+\frac{\pi}{4\mu_2}\frac{\partial P_2}{\partial x}\left(\kappa^4-\lambda^2\kappa^2\right)+\frac{\pi\kappa^4}{2\mu_2}\left(\frac{\partial P_2}{\partial x}-\frac{\partial P_1}{\partial x}\right)\ln\frac{\lambda}{\kappa} \tag{9}$$

$$Q_2=2\pi\int_{\kappa}^{\lambda}u_1rdr=-\frac{\pi}{4\mu_2}\left(\frac{\lambda^4}{2}-\kappa^2\lambda^2+\frac{\kappa^4}{2}\right)\frac{\partial P_2}{\partial x}+\frac{\pi\kappa^2}{4\mu_2}\left(\frac{\partial P_2}{\partial x}-\frac{\partial P_1}{\partial x}\right)\left[\lambda^2+2\kappa^2\left(\ln\frac{\kappa}{\lambda}-\frac{1}{2}\right)\right] \tag{10}$$

At this point, the volume flux of non-wetting phase Q_1 expression has three unknowns, the pressure gradients of both phases ($\partial P_1/\partial x$, $\partial P_2/\partial x$) and the interface position κ. Then, to reduce the number of variables, Eq. (7) is substituted in Eqs. (9) and (10). The resulting expressions of the volume flux where P_1 does not appear anymore, are written in the continuity equation (Eq. 5), which is solved for $\partial P_2/\partial x$:

$$\frac{\partial P_2}{\partial x}=\frac{Q}{\frac{\pi}{8}\left(\frac{\kappa^4-\lambda^4}{\mu_2}-\frac{\kappa^4}{\mu_1}\right)}+\frac{\sigma\left(\frac{1}{\kappa^2}\frac{\partial\kappa}{\partial x}+\frac{\partial^3\kappa}{\partial x^3}\right)\left(\frac{2\left(\kappa^4-\kappa^2\lambda^2\right)}{\mu_2}-\frac{\kappa^4}{\mu_1}\right)}{\left(\frac{\kappa^4-\lambda^4}{\mu_2}-\frac{\kappa^4}{\mu_1}\right)} \tag{11}$$

In such a way, we have the pressure gradient equations [Eqs. (7) and (11)], in which only the interface position κ is the unknown variable. These equations are written in Eq. (9), so Q_1 is now expressed explicitly through the interface position κ:

$$Q_1=\frac{Q\left[\frac{2\left(\kappa^4-\kappa^2\lambda^2\right)}{\mu_2}-\frac{\kappa^4}{\mu_1}\right]}{\left(\frac{\kappa^4-\lambda^4}{\mu_2}-\frac{\kappa^4}{\mu_1}\right)}+\frac{\pi}{8}\sigma\kappa^2\left(\frac{\partial\kappa}{\partial x}+\kappa^2\frac{\partial^3\kappa}{\partial x^3}\right)\left[\frac{\kappa^4\left(\frac{2\left(1-\frac{\lambda^2}{\kappa^2}\right)}{\mu_2}-\frac{1}{\mu_1}\right)^2}{\left(\frac{\kappa^4-\lambda^4}{\mu_2}-\frac{\kappa^4}{\mu_1}\right)}+\left(\frac{1}{\mu_1}+\frac{4}{\mu_2}\ln\frac{\lambda}{\kappa}\right)\right] \tag{12}$$

Finally, Eq. (12) is substituted in Eq. (8), closing the evolution equation. Nondimensionalizing in accordance with $\kappa^*=\kappa/R_T$, $r^*=r/R_T$, $x^*=x/R_T$, $\lambda^*=\lambda/R_T$, $\delta^*=\delta/R_T$, $L=\ell/R_T$, $\tau=t/(\mu_1R_T/\sigma)$, $Ca=Q/(\sigma\pi R_T^2/\mu_2)$, $P^*=P/(\sigma/R_T)$, the evolution equation in its dimensionless form is obtained:

$$\frac{\partial\kappa^*}{\partial\tau}=-\frac{Ca}{2\kappa^*}\frac{\partial}{\partial x^*}\left[\frac{1+2\frac{\mu_1}{\mu_2}\left(\frac{\lambda^{*2}}{\kappa^{*2}}-1\right)}{\frac{\lambda^{*4}}{\kappa^{*4}}+\frac{\mu_2}{\mu_1}-1}\right]+\left(\frac{1}{4\kappa^*}\right)\frac{\partial}{\partial x^*}\left[\begin{array}{l}\left(\kappa^{*2}\frac{\partial\kappa^*}{\partial x^*}+\kappa^{*4}\frac{\partial^3\kappa^*}{\partial x^{*3}}\right)\\ \left\{\frac{\left(\frac{\lambda^{*2}}{\kappa^{*2}}-1\right)\left[\left(\frac{\mu_1}{\mu_2}-\frac{1}{4}\right)\frac{\lambda^{*2}}{\kappa^{*2}}+\frac{3}{4}-\frac{\mu_1}{\mu_2}\right]}{\frac{\lambda^{*4}}{\kappa^{*4}}+\frac{\mu_2}{\mu_1}-1}-\right.\\ \left.\frac{\mu_1}{\mu_2}\ln\frac{\lambda^*}{\kappa^*}\right\}\end{array}\right] \tag{13}$$

The model representing Eq. (13) describes the evolution of the interface radius κ^* over time τ (dimensionless) for an imposed capillary number Ca, and includes the impacts of the rheology on the dynamics. In our simulations it is considered that when the interface radius reaches a value very close to the axial axis (x^*) at any point, it indicates the theoretical instant in which snap-off occurs. Equation (10) was solved, following Beresnev and Deng (2010), using a semi-discretization finite difference method known as Method of Lines (Schiesser, 1991), which is implemented in MATHEMATICA® (Knapp, 2008). The solution consider periodic boundary conditions, in

which it is assigned that the interface radius is equal at the boundaries for all simulation time, that is, $\kappa^*(-L/2, \tau)=\kappa^*(L/2, \tau)$. A uniform thickness of the wetting film δ^* was considered throughout the capillary wall as an initial condition (see Fig. 1); which was calculated using the fitting made by Deng *et al.* (2015) of Beresnev *et al.* (2011b) experimental data. This fitting was established as a function of the local capillary number as $\delta^*=0.0412\log_{10}(Ca)+0.1475$, and is valid in the range of $3\times10^{-4} \leq Ca \leq 1\times10^{-2}$. In the simulations presented here, we explored the same ranges of dimensionless geometric variables that Deng *et al.* (2015) did, namely: $2 \leq L \leq 16$ and $0.20 \leq a \leq 0.50$. The maximum dimensionless simulation time was also established in $\tau_{max}= 2\times10^5$.

2.3 Grouping of Values of Ca_{lim} by $\tilde{\alpha}$

The viscous forces predominate over the superficial ones at high capillary number flows. Due to this, the force that drives the flow of the wetting phase towards the constriction tends to disappear and thereby inhibits the snap-off. Peña *et al.* (2009) observe that under limit conditions, that is, $Ca\rightarrow\infty$, $\sigma/(Q/\pi R_T^2)\mu_2\rightarrow0$, "*There should be a finite critical value of capillary number above which the viscous stress at the wall is stronger than the capillary driven flow and snap-off is not observed*".

As already mentioned, Deng *et al.* (2015) conducted a numerical study analyzing the existence of an local capillary number upper limit in which the snap-off is inhibited, even if the static breakup criteria are met. This local capillary number limit can be obtained with the aid of the model that represents Eq. (13). If this model is evaluated starting from the lower limit $Ca=3\times10^{-4}$, given values of length L and radii ratio a that meet the static breakup criteria, it is expected that the snap-off will occur; but when Ca increases, a critical value of Ca where the breakup is inhibited exists. This upper limit is called $Ca_{\lim}$.

The values of Ca_{lim} for various combinations of dimensionless lengths L, radii ratios a, and for a viscosity ratio $k = \mu_1/\mu_2 =1$, obtained by Deng *et al.* (2015) by following a similar procedure to the one above, are shown in Fig. 2. In this figure, the Ca upper limits shows a singular behavior for a specific value of a: the Ca_{lim} increases and then decreases as L increases. This behavior can be interpreted by the competition between the imbalance in the capillary pressure and the wetting phase travel time from the crest to the throat; since both increase as L grows. For example, the increase of the capillary pressure difference has a quadratic dependence on L (see Beresnev *et al.* 2009; Eq. 5). Moreover, for an L value given, as the radii ratio decreases the imbalance in the capillary pressure increases, while the breakup times (therefore those of travel) are reduced (see Deng *et al.* 2015; Fig. 4). Consequently, for lower values of a, Ca_{lim} increases.

According to the results listed above, the behavior of the critical conditions of the Ca depends on the combination of the geometrical parameters (length and radii ratio); so that a relationship between these critical conditions of the flow dynamics and an integral form of the geometry, in this case the geometric gradient $\tilde{\alpha}$, was sought to be established.

It should be noted that the value of $\tilde{\alpha}$ is not exclusive of a single geometric configuration, that is, different combinations of a and L result in a same value of $\tilde{\alpha}$. For example, values of L={16, 15, 14,…, 10} and a={0.20, 0.25, 0.30,…, 0.50}, are grouped in □=0.10. Thus, for this study n groups of geometric configurations were defined to cover the range of both geometric variables, where each group is represented by a value of $\tilde{\alpha}$. For each group of geometric configurations, the corresponding associated values of $Ca_{lim}^{\tilde{\alpha}}$ were obtained using the model of Eq. (13). As it was intuitively predicted, these values of $Ca_{lim}^{\tilde{\alpha}}$, being grouped by $\tilde{\alpha}$, have some relation with the pore geometry, in such a way that they fit properly if a linear model of the form $Ca_{lim}^{\tilde{\alpha}}=m_iL+b_i$ is used; where m_i and b_i are fitting parameters. In Fig. 2, for example, the fitting straight lines of $Ca_{lim}^{\tilde{\alpha}}$ are shown for the groups of geometric configurations corresponding to $\tilde{\alpha}_{i,j,k}$={0.125,0.105,0.088}, which coincide with the values of Ca_{lim} obtained by Deng *et al.* (2015). Moreover, the values of the coefficients that take the whole set of linear relations of the type $Ca_{lim}^{\tilde{\alpha}}=m_iL+b_i$ follow a power law with $\tilde{\alpha}_i$: $m_i=d\tilde{\alpha}_i^e$ and $b_i=f\tilde{\alpha}_i^g$, where the fitting parameters are d, e, f and g.

Based on the exposed linear behavior and the empirical relationships, we present an expression to reproduce the family of curves of Ca_{lim} as a function of the capillary geometry and four fitting parameters:

$$Ca_{\lim} = d\tilde{\alpha}^eL + f\tilde{\alpha}^g \qquad (14)$$

In the determination of the parameters of the best fitting for the model of Eq. (14), the method known as *Differential Evolution* (Storn and Price, 1997) was considered, where the objective function was established as a least squares optimization problem:

$$\min E(x) = (1/2)\sum_{i=1}^{M}\left[\widehat{Ca}_{\lim} - Ca_{\lim}(\psi)\right]^2 \qquad (15)$$

given the correspondence: ψ={d, e, f, g}.

In Fig. 2 is shown the comparison of the Ca_{lim} values obtained by Deng *et al.* (2015), and those obtained from the fitting of Eq. (14), for a viscosity ratio equal to unity; in this figure the vertical left lines were determined by the quasistatic criterion (Deng *et al.* 2015).

2.4 Attribution of Viscosity Ratio k in Ca_{lim}

In the case of arbitrary viscosities of the fluids, shear stress at the interface, which resists the continuous phase flow, exists and increases with the viscosity ratio. For this reason, the snap-off might not occur at certain values of viscosity ratio. In order to know the effect of the viscosity ratio on the Ca_{lim} behavior, a series of simulations of the drop breakup model [Eq. (13)] was performed amongst a range of $0.75 \leq k \leq 20$.

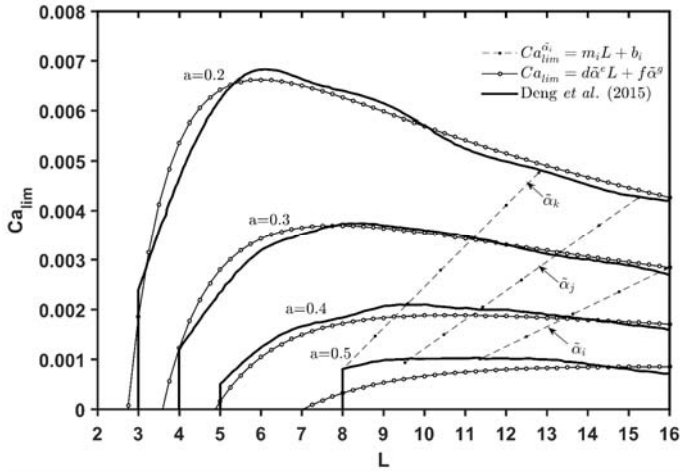

Fig. 2. Local capillary number upper limits (*Ca*$_{lim}$) in which the snap-off is inhibited, given a porous length *L* and pore radii ratio *a*; for a viscosity ratio *k*=1.00.

Figure 3 shows the *Ca*$_{lim}$ behavior for *a*=0.20 and different combinations of viscosity ratio while Fig. 4 shows the *Ca*$_{lim}$ values by fixing the *k* value and by varying the radii ratio. From Figs. 3 and 4. it can be seen that the *Ca*$_{lim}$ follows a general trend for all the range of values. It is important to notice that as the *k* value increases, the increase of *Ca*$_{lim}$ values starting from the left boundary becomes increasingly smoother, as can be seen in Fig. 3. The decrease in *Ca*$_{lim}$, starting from its maximum point, is more pronounced as *k* grows. Even right boundaries begin to appear starting from moderately high *k* values. In the series of graphs of Fig. 4, it is worth noting that the range of radii ratio in which snap-off occurs under dynamic conditions is constrained by the increment of the viscosity ratio *k*. For example, for *k*=1.50 and *a*=0.5 there are no values of *Ca*$_{lim}$ at any length, i.e., drop breakup, given these conditions, can only occur for static conditions.

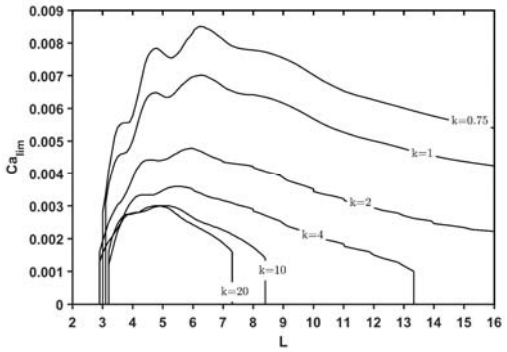

Fig. 3. *Ca*$_{lim}$ values for a radii ratio *a*=0.2 and different viscosity ratios.

These descriptions of the effect of the viscosity ratio *k* on the *Ca*$_{lim}$ values shown in Figs. 3 and 4, coincide in that an increase of *k* invariably leads to a decrease of the cases in which snap-off occurs; either in a lower range of pore lengths *L*, radii ratio *a* or capillary numbers *Ca*.

2.5 Effect of *Ca* and *k* on Snap-off Time

In this section, the effect of the viscosity ratio *k* in the dimensionless snap-off time τ_s for different geometric configurations and *Ca* values is analyzed. Here, the dimensionless snap-off time τ_s is defined as the elapse of time between the start of the simulation, initial conditions being established, and the instant in which the snap-off occurs.

For this analysis, first the model was evaluated for a fixed geometry (*L*=10, *a*=0.20), equal viscosity of the phases ($\mu_1=\mu_2 \rightarrow k=1$), and *Ca* was slowly increased from its inferior limit ($Ca=3\times10^{-4}$) until it reached the *Ca*$_{lim}$. The same procedure was repeated for other viscosity ratios. In each simulation τ_s was obtained. These results are illustrated in Fig. 5, which shows the effect of *Ca* and *k* in snap-off time, given a geometry. Similarly, families of curves for different viscosity ratios *k* were obtained (Fig. 6). For each family of curves *k* and *L* remains fixed, and different radii ratios are evaluated.

At first inspection, it can be noticed that the graphs in Figs.5 and 6 vary meaningfully from the snap-off time lineal behavior observed for foams (Gauglitz and Radke,1990; Fig. 11). The general behavior of the curves shown in Figs. 5 and 6 is characterized for presenting the maximum value of τ_s for the minimum value of *Ca*. This value gradually decreases as *Ca* increases, but is interrupted by the sudden rise of τ_s. After this rise, τ_s continues to decrease in other *Ca* range of values, until an increase is presented again. This behavior is repeated, until the *Ca*$_{lim}$ is reached. As reported by Deng *et al*. (2015) [Fig. 5], the τ_s sudden increase is due to the snap-off position migration.

The most notable effect of viscosity ratio in the snap-off time is shown in Fig. 5. In this figure, the increase in the viscosity ratio *k* tends ¨to compress¨ the snap-off time curves. The curves maintain their characteristic behavior as there is a greater *k* value, but the *Ca* upper limit decreases. In other words, the increase in the viscosity ratio causes the snap-off change position to occur in *Ca* intervals

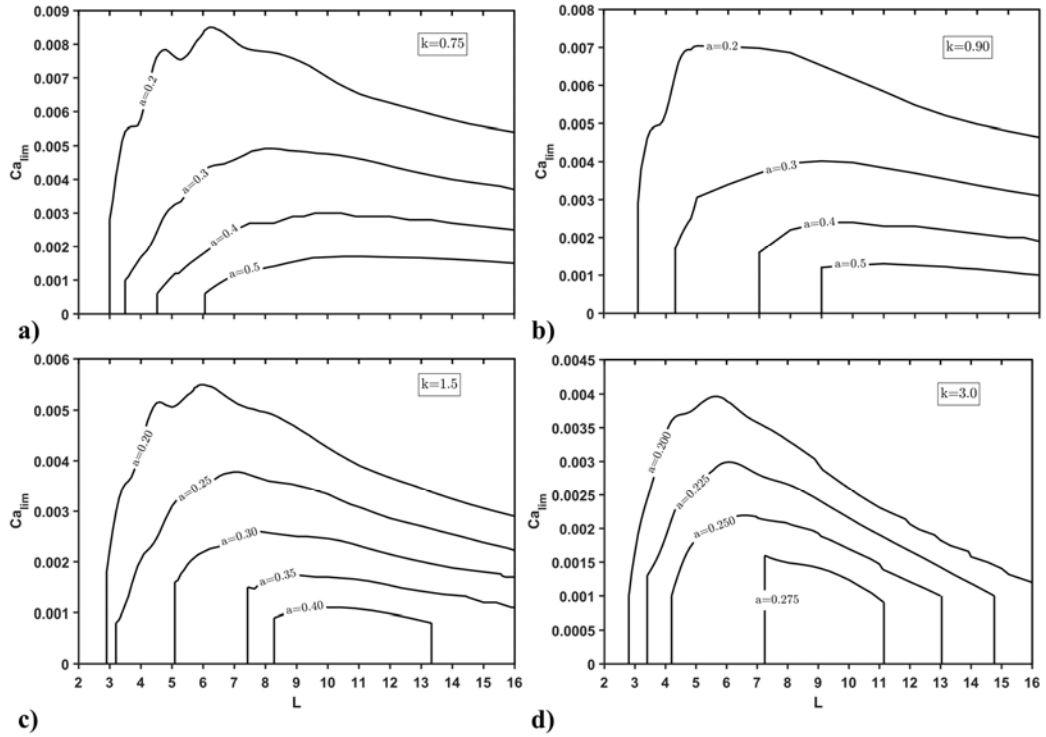

Fig. 4. Families of Ca_{lim} curves for different viscosity ratios a) k=0.75 b) k=0.90 c) k=1.5 d) k=3.0.

increasingly minor. Thus, the τ_s range segments tend to be shorter. It should be pointed out that for the same *Ca* value, the τ_s can be augmented or diminished with the viscosity ratio, without an existent tendency; therefore, the τ_s curves at some points cross one another. The foregoing does not occur in the graphs shown in Fig. 6. In this figure, two behaviors are distinguished with respect to the radii ratio increase: 1) that snap-off time increase reflect the dependency of the wetting phase travel time, and consequently snap-off time with the geometry 2) the *Ca* value range decreases for each curve, which is consistent with the Ca_{lim} behavior shown in Figs. 2 and 4, and discussed above.

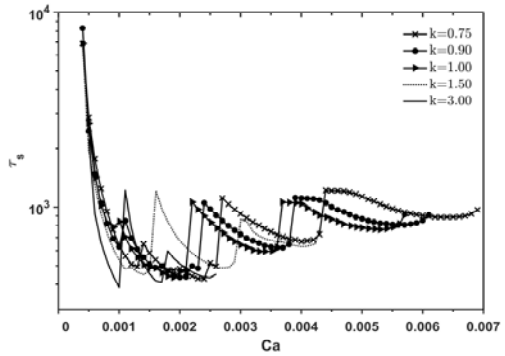

Fig. 5. Snap-off time for for different k and *Ca* values. L=10, a=0.20.

3. RESULTS AND DISCUSSION

The methodology presented in this study is based on the grouping of Ca_{lim} values, which were obtained through Eq. (13), linked to a same geometric gradient value $\tilde{\alpha}$, and its subsequent fitting to an empirical model represented by Eq. (14). This methodology was used to reproduce the family of Ca_{lim} curves for viscosity ratios different from the unity. Table 1 shows the values of the fitting parameters and those that the objective function acquires after the optimization process, for different values of k.

On the other hand, well-defined trends of the fitting parameters (see Table 1) in relation to k were detected, for example, of logarithmic type; allowed establishing a general model, with few parameters, of the local capillary number upper limit in terms of the capillary geometry and viscosity ratio:

$$Ca_{\lim}^{k} = \beta\tilde{\alpha}^{2}\left[\tilde{\alpha}^{\eta}L - C\tilde{\alpha}^{\eta+D}\right] \tag{16}$$

where $\beta=Ak+B$ and $\eta=\ln(k^{0.5})$. The fitting parameters are then $\Psi=\{A, B, C, D\}$; which, after applying the optimization algorithm, taken the values: $\Psi=\{0.0039,0.0586,1.8945,-0.6667\}$.

The results of the error function $E1(\Psi)$, analogous to Eq. (15) but taking into account Eq. (16), are shown in Table 1. Fig. 7 illustrates the Ca_{lim} behavior from Eqs. (14) and (16) using the parameters of Table 1, which are also compared with the Ca_{lim} values from Eq. (13). For reader's conveniences, in Fig. 7 is included a simplified diagram of the capillary with the main geometric variables in dimensionless form. Here, the interface has reached a value close to zero in one of its point; situation that does not occur in the cases in which Ca_{lim} is exceeded, where the interface reach an equilibrium position close to the initial condition.

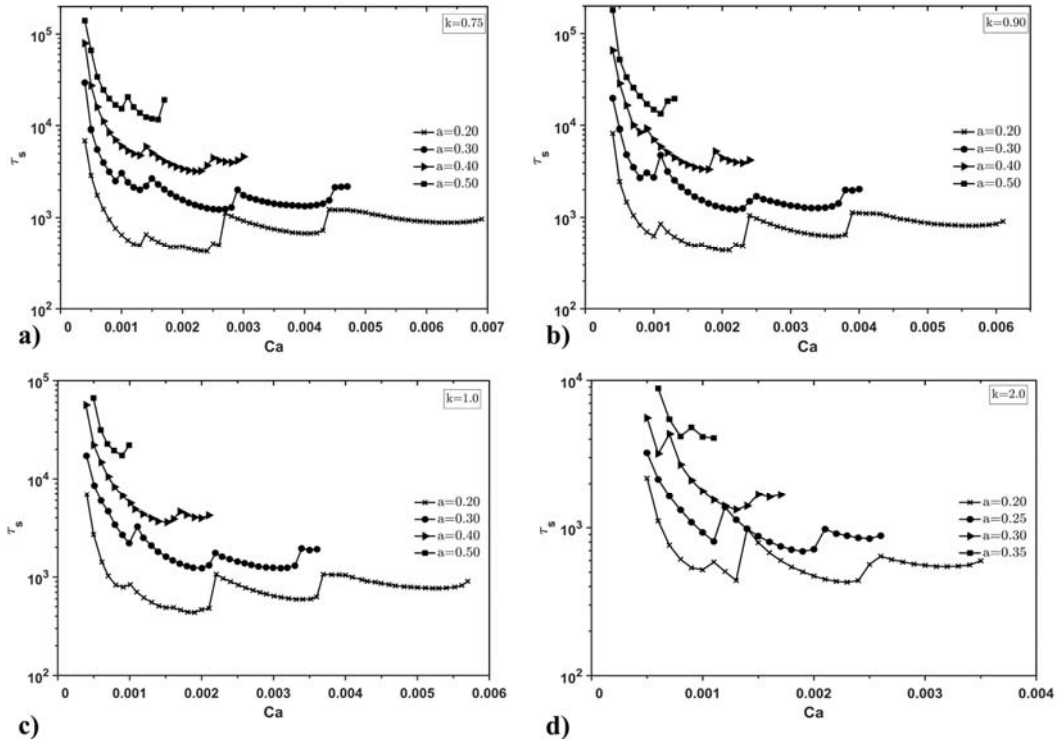

Fig. 6. Snap-off time families curves for different viscosity ratios a) *k*=0.75 b) *k*=0.90 c) *k*=1.0 d) *k*=2.0. *L*=10.

Table 1 Values of the fitting coefficients and the objective functions[a]

k_i	$\psi_i=\{d_i, e_i, f_i, g_i\}$	$E(\psi_i)$	$E1(\Psi)$
0.75	0.0698, 1.9781, 0.1349, 1.3443	2.13 E-5	3.94 E-5
0.90	0.0661, 1.9928, 0.1244, 1.3233	7.91 E-6	9.50 E-6
1.00	0.0793, 2.1209, 0.1518, 1.4593	8.93 E-6	1.41 E-5
1.50	0.0888 , 2.2411, 0.1620, 1.5001	3.80 E-6	1.18 E-5
2.00	0.1091, 2.4070, 0.1974,1.6383	2.48 E-6	1.26 E-5
2.50	0.1294, 2.5263, 0.2302, 1.7269	3.31 E-6	1.25 E-5
3.00	0.1408 , 2.5991, 0.2483, 1.7836	3.41 E-6	1.51 E-5
3.50	0.1381, 2.6149, 0.2412, 1.7869	3.77 E-6	1.55 E-5
4.00	0.1358, 2.6376, 0.2364, 1.8055	3.91 E-6	1.23 E-5
4.50	0.1116, 2.6195, 0.1961, 1.8071	3.95 E-6	8.33 E-6
10.0	0.3492, 3.1809, 0.5983, 2.2977	3.52 E-7	4.39 E-6
20.0	0.3424, 3.4302, 0.6009, 2.5870	2.91 E-7	3.87 E-6

[a] $\Psi=\{0.0039,0.0586,1.8945,-0.6667\}$. Read 2.13 E-5 as 2.13×10^{-5}.

As can be seen in the results of Fig. 7, the models of the Eqs. (14) and (16) adequately reproduce the Ca_{lim} behavior in the range of the physical variables of study and can serve as breakup criteria if it is established that:

$$Ca < Ca_{\lim}\left(a, L, \psi_i\right) \tag{17}$$

if Eq. (14) is considered; or

$$Ca < Ca_{\lim}\left(a, L, k, \Psi\right) \tag{18}$$

when Eq. (16) is chosen.

Examining the results showed in Fig. 7, it can be seen that better approximations of the Ca_{lim} values [calculated with Eq. (13)] are obtained if an equation of the form Eq. (14) is used, in which the parameter value varies for each *k*; that those resulting from applying a fixed parameter fitting for the entire range of viscosity ratios [Eq. (16)]. However, in spite of its limitations, this last fitting equation reproduces in an acceptable way the behavior of the family of Ca_{lim} curves. This can be verified by comparing the values that the objective function reaches. Table 1 confirms that the global error increases, in the worst case, in an order of magnitude.

Although the mathematical fitting applied to estimate the Ca_{lim} value as a function of the capillary geometry and the viscosity ratio is empirical, it should be noticeable that the physics of the phenomenon being studied is well represented in the Ca_{lim} graphs. The models represented in Fig. 7, as will be discussed in the following paragraphs, express the behavior of the snap-off involving the three forces that regulate this mechanism: the capillary pressure difference that drives the wetting

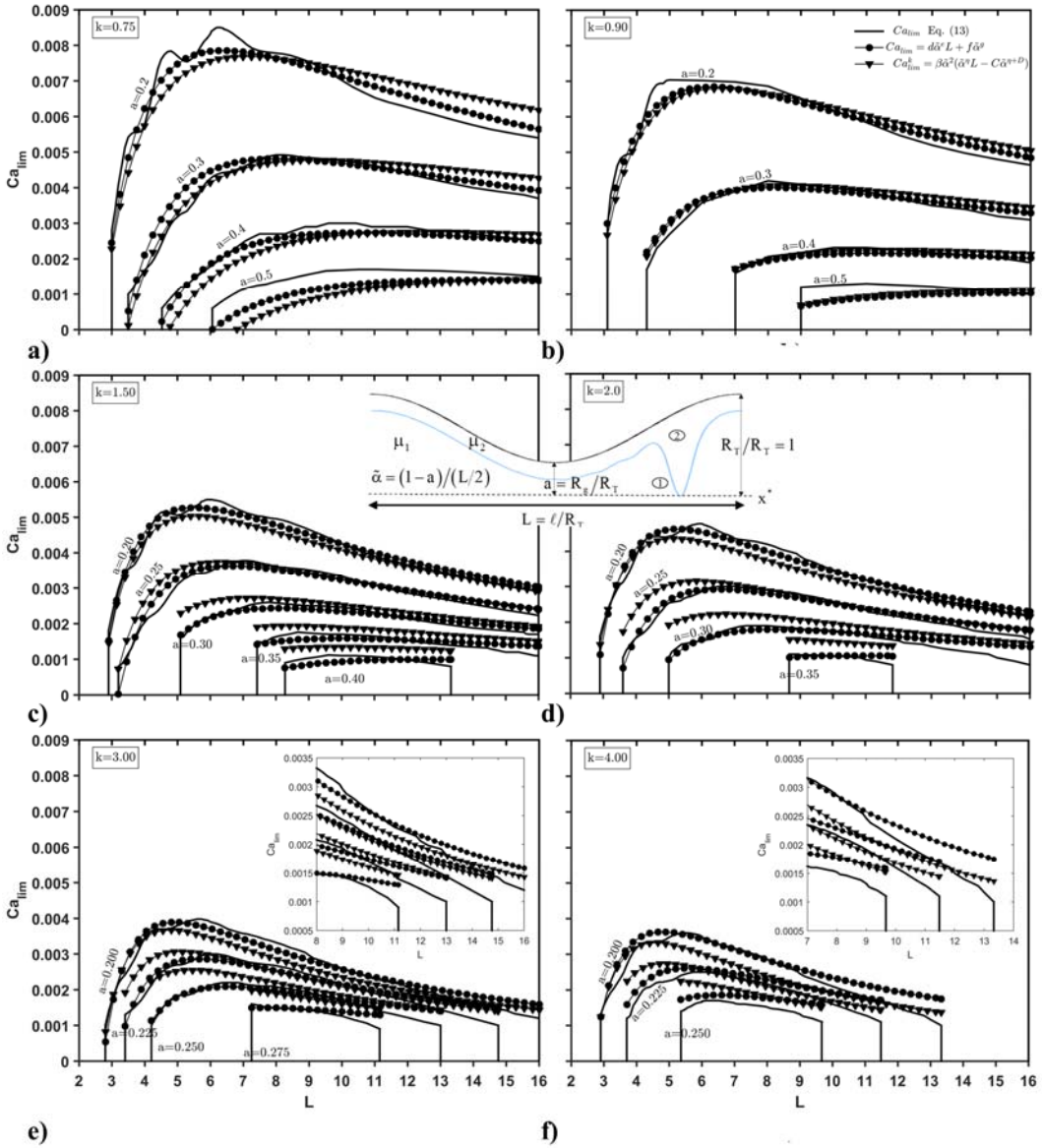

Fig. 7. Families of Ca_{lim} curves obtained with different models: 1) —— from Eq. 13 (Beresnev and Deng, 2010) 2) —●— $Ca^{\tilde{\alpha}}_{lim} = d\tilde{\alpha}^e L + f\tilde{\alpha}^g$ 3) —▼— $Ca^{k}_{lim} = \beta\tilde{\alpha}^2\left[\tilde{\alpha}^\eta L - C\tilde{\alpha}^{\eta+D}\right]$.

phase to constriction, the flow resistance of the wetting liquid and the squeezing process of the non-wetting phase. These forces are modified as the pore geometry $\tilde{\alpha}=(R_T-R_g)/(\ell/2)$, the viscosity ratio $k=\mu_1/\mu_2$, and the capillary number $Ca=(Q/\pi R_T^2)\mu_2/\sigma$, vary.

As to the capillary pressure difference at the crest and at the constriction, present at the beginning of the snap-off process, it is known that this depends on the difference in the curvature of the interface profile. Since an initial condition of the wetting film parallel to the pore wall and coupled with the local capillary number was established, the capillary pressure difference has a direct relationship with *Ca* and the geometry. In fact, the Beresnev *et al*. (2009) static breakup criterion comes from the condition $P_c^{throat} > P_c^{crest}$, for snap-off occurs. After a series of algebraic operations, this condition can be written in terms of the geometry and the local capillary number as:

$$L > 2\pi\sqrt{\left(1-\delta^*\right)\left(a-\delta^*\right)} \tag{16}$$

where $\delta^*=0.0412\log_{10}(Ca)+0.1475$.

This criterion is fulfilled in all cases evaluated here, even if it is evaluated at the maximum value of *Ca* analyzed ($Ca=1\times10^{-2}$). However, for dynamic flow conditions the capillary driven flow will no longer be the only determining force in the breakup, so this criterion is no longer valid. Although, as shown in Fig. 2, $\tilde{\alpha}$ retains some influence on the Ca_{lim} behavior, for example, we have that for a same value of $\tilde{\alpha}$, the upper limit of the local capillary number will grow (linearly) as the length increases and the radii ratio decreases.

On the other hand, if the viscosity of the wetting phase (μ_2) is fixed, the increase in the viscosity ratio $k=\mu_1/\mu_2$ will occur as the viscosity of the non-wetting phase (μ_1) increases. Under these conditions, the flow of the wetting phase towards the constriction decreases due to the increase of the shear stress and the squeezing process of the non-wetting phase. This situation becomes worse at high capillary numbers, where viscous forces predominate over the superficial ones. Then, it could be expected that as the viscosity ratio increases, the wetting-phase collar present in the constriction when the snap-off occurs, will not reach the development for high capillary numbers. This response can be verified if are compared, for example, the graphs a) k=0.75 and f) k=3.0 of Fig. 7. Particularly in the Fig. 7f, the viscosity ratio has been increased four times in relation to the first case (Fig. 7a), in which it is evident that the range of values in which snap-off occurs has decreased.

4. CONCLUSION

A numerical analysis of the capillary number upper limit (Ca_{lim}), in which the snap-off is inhibited, was performed aiming to establish a dynamic breakup criterion that, unlike the static criteria, would include: some aspects of rheology of the two-phase system, such as the viscosity ratio; the dynamic factors of the flow, encapsulated in the local capillary number; and an integral form of the capillary geometry, represented by a parameter that relates both radii and the distance between them.

As discussed throughout this paper, the critical conditions of occurrence of the snap-off involve a complex combination of competitive forces that vary as the physical variables of study are modified. Although observing that geometry determines certain general behaviors of Ca_{lim}, the possibility of relating an integral form of this one with the inhibition of the drop breakup phenomenon in flows at high capillary number was explored. This idea resulted in a linear clustering of the upper limit values of the capillary number, associated with the same $\tilde{\alpha}$ value, with the respective lengths; which served as the basis of the series of mathematical fittings presented here to estimate Ca_{lim} as a function of pore geometry and viscosity ratio.

The numerical solution of the snap-off phenomenon was established from a dynamic drop breakup model [Eq. (13)] proposed and validated by Beresnev and coworkers. In principle, this model represents by itself a dynamic breakup criterion that includes the mentioned variables. However, the solution of the model, described by a highly nonlinear partial differential equation of fourth order, is not an easy task, so it is not feasible to use it as such. In fact, implementing it, for example, in pore network models would result in high computational costs. In contrast, the simple formulations proposed here have the following advantages: 1) they adequately relate the main physical variables of the system with the inhibition of the drop breakup 2) their behavior agrees with the theoretical explanations of snap-off occurrence based on the competition of forces that occurs in the liquid phases 3) can be implemented easily on other models.

As mentioned before, the smaller slope wall ($\alpha=2/L\ll1$) and the capillary number, the better the small-slope approximation is. Here, the model was evaluated for a range of relative small Ca ($3\times10^{-4} \leq Ca \leq 1\times10^{-2}$), but also, in some cases for small dimensionless lengths L where $\alpha\approx1$. In these limit cases, some instabilities in the graphs of Ca_{lim} behavior can be appreciated (see Figs. 3 and 4). Thus, the model is expected to fail if the limits of the small-slope approximation are exceeded.

The analysis of the snap-off dynamics presented here was restricted to pure interfaces. Future research might focus on the study of drop breakup criteria for complex rheological behaviors, such as the viscoelastic interfacial stress analyzed by Hoyer *et al*. (2016) in the context of the snap-off.

ACKNOWLEDGEMENTS

The first author is grateful for the financial support from the doctoral grants of the National Council for Science and Technology (CONACyT) in Mexico (Grant No. 253645).

REFERENCES

Alvarado, V., M. Moradi, G. Garcia Olvera, B. Morin and J. Oakey (2014). Interfacial visco-elasticity of crude oil-brine: An alternative EOR mechanism in smart waterflooding. In *SPE Improved Oil Recovery Symposium,* Tulsa, OK, USA.

Beresnev, I. and W. Deng (2010). Theory of breakup of core fluids surrounded by a wetting annulus in sinusoidally constricted capillary channels. *Physics of Fluids (1994-present)* 22(1), 012105.

Beresnev, I., W. Gaul and R. D. Vigil (2011a). Forced instability of core-annular flow in capillary constrictions. *Physics of Fluids (1994-present)* 23(7), 072105.

Beresnev, I., W. Gaul and R. D. Vigil (2011b). Thickness of residual wetting film in liquid-liquid displacement. *Physical Review E* 84(2), 026327.

Beresnev, I., W. Li and R. D. Vigil (2009). Condition for break-up of non-wetting fluids in sinusoidally constricted capillary channels. *Transport in Porous Media* 80(3), 581-604.

Blunt, M. J., Bijeljic, B., Dong, H., Gharbi, O., Iglauer, S., Mostaghimi, Paluszny, A. and Pentland, C. (2013). Pore-scale imaging and modelling. *Advances in Water Resources* 51, 197-216.

Cobos, S., M. Carvalho and V. Alvarado (2009). Flow of oil–water emulsions through a constricted capillary. *International Journal of Multiphase Flow* 35(6), 507-515.

Deng, W., M. Balhoff and M. B. Cardenas (2015). Influence of dynamic factors on nonwetting fluid snap‐off in pores. *Water resources*

research 51(11), 9182-9189.

Gauglitz, P. and C. Radke (1990). The dynamics of liquid film breakup in constricted cylindrical capillaries. J*ournal of Colloid and Interface Science* 134(1), 14-40.

Guillén, V. R., M. I. Romero, M. Carvalho, and V. Alvarado (2012b). Capillary-driven mobility control in macro emulsion flow in porous media. *International Journal of Multiphase Flow* 43, 62-65.

Guillén, V., M. Carvalho and V. Alvarado (2012a). Pore scale and macroscopic displacement mechanisms in emulsion flooding. *Transport in Porous Media* 94(1), 197-206.

Hoyer, P., V. Alvarado and M. Carvalho (2016). Snap-off in constricted capillary with elastic interface. *Physics of Fluids (1994-present)* 28(1), 012104.

Knapp, R. (2008). A Method of Lines Framework in Mathematica. *JNAIAM* 3(1-2), 43-59.

Kokal, S. L. (2005). Crude Oil Emulsions: A State-Of-The-Art Review. *SPE Production & Facilities* 20(01), 5-13.

Kovscek, A. and C. Radke (1996). Gas bubble snap-off under pressure-driven flow in constricted noncircular capillaries. *Colloids and Surfaces A: Physicochemical and Engineering Aspects* 117(1), 55-76.

Kovscek, A. and C. Radke (2003). Pressure-driven capillary snap-off of gas bubbles at low wetting-liquid content. *Colloids and Surfaces A: Physicochemical and Engineering Aspects* 212(2), 99-108.

Kovscek, A., G. Q. Tang, and C. Radke (2007). Verification of Roof snap off as a foam-generation mechanism in porous media at steady state. *Colloids and Surfaces A: Physicochemical and Engineering Aspects* 302(1), 251-260.

Peña, T., M. Carvalho and V. Alvarado (2009). Snap‐off of a liquid drop immersed in another liquid flowing through a constricted capillary. *AIChE journal* 55(8), 1993-1999.

Romero, M. I., M. Carvalho and V. Alvarado (2011). Experiments and network model of flow of oil-water emulsion in porous media. *Physical Review E* 84(4), 046305.

Roof, J. (1970). Snap-off of oil droplets in water-wet pores. *Society of Petroleum Engineers Journal* 10(01), 85-90.

Rossen, W. R. (2000). Snap-off in constricted tubes and porous media. *Colloids and Surfaces A: Physicochemical and Engineering Aspects* 166(1), 101-107.

Rossen, W. R. (2008). Comment on "Verification of Roof snap-off as a foam-generation mechanism in porous media at steady state". *Colloids and Surfaces A: Physicochemical and Engineering Aspects* 322(1), 261-269.

Schiesser, W. E. (1991). *The Numerical Method of Lines: Integration of Partial Differential Equations*. Academic Press, San Diego, USA.

Storn, R. and K. Price (1997). Differential evolution–a simple and efficient heuristic for global optimization over continuous spaces. *Journal of Global Optimization* 11(4), 341-359.